Martin Seiß | Frank Spahn

Hydrodynamics of Saturn's Dense Rings

Suggested citation referring to the original publication:
Mathematical Modelling of Natural Phenomena 6 (2011) 4, pp. 191-218
DOI https://doi.org/10.1051/mmnp/20116409
ISSN (print) 0973-5348
ISSN (online) 1760-6101

Math. Model. Nat. Phenom.
Vol. 6, No. 4, 2011, pp. 191-218
DOI: 10.1051/mmnp/20116409

Hydrodynamics of Saturn's Dense Rings

M. Seiß[*] and F. Spahn

Department of Physics and Astronomy, University of Potsdam, D-14476 Potsdam, Germany

Abstract. The space missions Voyager and Cassini together with earthbound observations revealed a wealth of structures in Saturn's rings. There are, for example, waves being excited at ring positions which are in orbital resonance with Saturn's moons. Other structures can be assigned to embedded moons like empty gaps, moon induced wakes or S-shaped propeller features. Furthermore, irregular radial structures are observed in the range from 10 meters until kilometers. Here some of these structures will be discussed in the frame of hydrodynamical modeling of Saturn's dense rings. For this purpose we will characterize the physical properties of the ring particle ensemble by mean field quantities and point to the special behavior of the transport coefficients. We show that unperturbed rings can become unstable and how diffusion acts in the rings. Additionally, the alternative streamline formalism is introduced to describe perturbed regions of dense rings with applications to the wake damping and the dispersion relation of the density waves.

Key words: granular gas, instabilities, hydrodynamics, planetary rings
AMS subject classification: 35Q35, 70F15, 70F07

1. Introduction

The planet Saturn owns the most impressing and largest ring complex in our solar system. All outer planets are girdled by a ring system, but these are not as large and bright as the rings of Saturn. The latter consist of the inner dense main rings and the outer faint rings. The outer rings are formed by micrometer sized icy dust particles with very low particle number density (< 1 m^{-3}). Thus, collisions between the particles are of minor importance and these rings are not suited for hydrodynamic applications.

[*]Corresponding author. E-mail: mseiss@uni-potsdam.de

This article will concentrate on the most massive rings of Saturn – the A and B ring. These dense regions have optical depths larger than 0.5, where the geometric optical depth is defined by

$$\tau = \int\int \pi R^2\, n(x, y, z, R)\; dz\, dR. \tag{1.1}$$

Here, $n(x, y, z, R)$ denotes the particle number density of the medium along the line of sight with R labeling the radius of the ring particles. The optical depth profile along the radial distance to Saturn is shown in figure 1 giving an estimate of the distribution of the surface mass density in the rings. The A and B ring are separated by the Cassini division with smaller densities ($\tau \approx 0.1$) than in the A and B ring. However, the Cassini division is similar to the C ring which orbits inside the B ring. All main rings – A, B and C ring and Cassini division – are dense enough to be collisionally dominated, and thus, are suited for a hydrodynamic description.

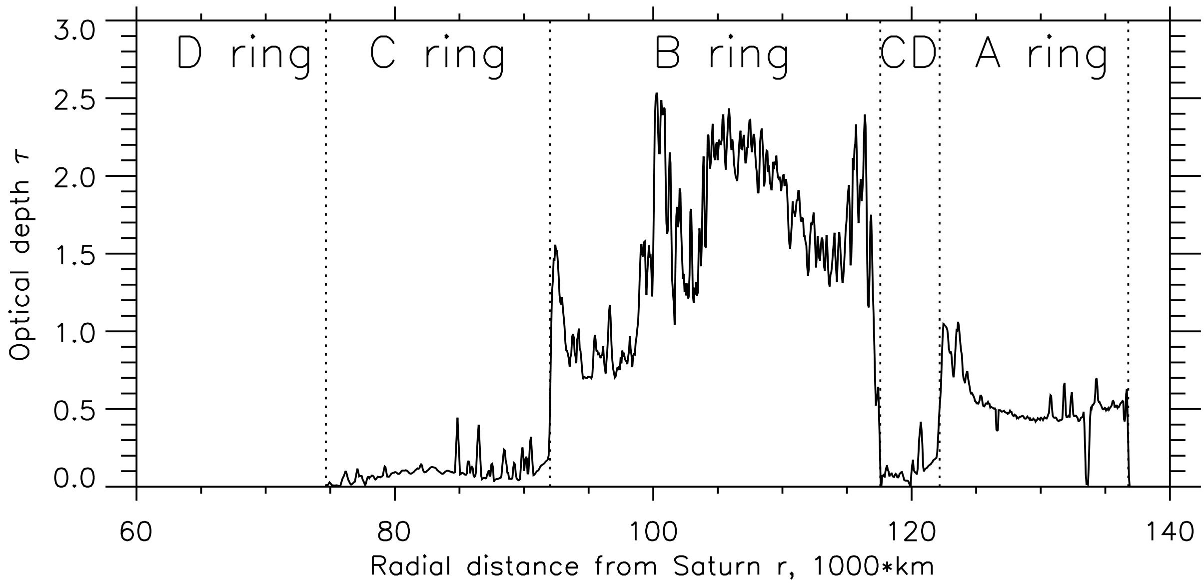

Figure 1: Optical depth profile from the Voyager PPS scan. The radius of Saturn exceeds 60,000 km. CD denotes the Cassini division.

Additionally, the ring system contains the innermost low density dusty D ring located between the C ring and Saturn's atmosphere consisting mainly of micrometer sized particles. Finally, the bizarre, faint and kinky F ring orbits outside the A ring and is formed by micrometer up to kilometer sized objects.

A wealth of structures in Saturn's rings has been puzzling scientists since decades. Here we will present some of them which can be understood in the context of hydrodynamical ring models. First, we will characterize the physical properties of the granular ring particle ensemble in section 2. In section 3. the basic hydrodynamic balance equations are introduced and we emphasize the peculiar behavior of the granular transport coefficients (section 3.). Next, we demonstrate that the unperturbed rings can become unstable and how diffusion acts in the rings. Finally, the streamline formalism is introduced for the description of perturbed rings with its applications to the wake damping and the dispersion relation of the density waves at resonances (section 4.). The latter density waves are a result of the interplay between ring gravity and tidal forces and provide a possibility to determine the ring mass.

2. A cosmic granular "gas" in orbit around Saturn

Saturn's rings generally consist of ice particles which are polluted by a small fraction of silicates. The size distribution of the particles in dense ring regions can be determined with the help of occultation experiments [82, 20, 27]. These observations indicate that the particle sizes can be modeled by a power law distribution $n(R) \approx n_0(R/R_0)^{-3}$ in the size range of several centimeters until tens of meters. The collective dynamics of the ring particles is mainly determined by a Kepler motion around the central planet and the small fluctuations caused by collisions between them. Perturbations induced by the moons of Saturn can alter this motion pattern of the particles leading to a formation of certain structures in the rings.

The collisions between ring particles are inelastic and characterized by a coefficient of restitution ϵ, which quantifies the dissipative decay of the relative velocities between the particles during the collisions ($\epsilon = 0$ for totally inelastic and $\epsilon = 1$ for elastic). The in-elasticity of the particles is crucial for the stability of the rings. Without dissipation the velocity dispersion of the particles would increase with each collision (viscous heating driven by shear) until the particles hit the surface of Saturn or escape the system. Thus, the rings would finally evaporate [29]. Several attempts have been made to quantify the coefficient of restitution on base of theoretical models [2, 7, 13, 1, 14] and experiments [12, 30, 32] – mainly confirming a decreasing coefficient of restitution with increasing collision velocity.

Beside restitution also fragmentation and coagulation play an important role [44, 15, 4, 64]. The observed ring particles are most probably agglomerates of smaller constituents and their distribution reflects the balance between coagulation and fragmentation. The particles form agglomerates because of the adhesive contact forces on one side [1, 14] and the particle self-gravity on the other [23, 80]. Smaller agglomerates (< 1m) are mainly hold together due to the adhesive surface forces (strength regime) whereas larger agglomerates are stabilized by their self-gravity [80, 1] (gravity regime). The particle agglomerates can be destroyed by collisions, tidal forces or meteoroid impacts.

However, coagulation and fragmentation will not be discussed further in this article and we will focus on the effect of the in-elasticity of the collisions. The particles move on Kepler orbits around the planet, which are nearly circular. The third Kepler law tells us that the inner particles move with higher mean velocities around the planet than the outer ones. Thus, a systematic shear flow induces a viscous friction which heats up the granular ensemble. This process is balanced by a cooling of the material due to the in-elasticity of the collisions and leads to a rather small velocity dispersion of the order $R\Omega$, where $\Omega = \sqrt{GM_s/a^3}$ denotes the Kepler frequency. The Kepler frequency depends on the gravitational constant G, the mass of Saturn M_s and the semi-major axis a of the particle. In addition, the shear flow implicates a non-isotropic velocity dispersion which is precisely described by a tensor. The velocity dispersion with mm/s and cm/s! is by a factor of 10^{-7}-10^{-8} smaller than the systematic Kepler flow – i.e. $R\Omega \ll a\Omega$ (nearly circular orbits), which is the reason one can speak about "cold" discs in the context of planetary rings.

Furthermore, the small velocity dispersion controls also the disc height H via $c \approx \Omega H$, and thus the ring has also a very small vertical extent of around 10 m (a few mean particle radii) in contrast to the ring diameter of the order 10^8 m. If one compares the disc height with the observed normal optical depth of the order of unity one has to conclude that the rings are rather densely packed systems. Thus, the mean free path of the particles is of the order of the particle radii. This can cause the particles to arrange vertically in more than one layers [81, 50], whereas in dilute systems the vertical density profile is well described by a Gaussian.

In the end of this introduction to the granular matter of planetary rings we will call attention to the fact that most parts of Saturn's A and B ring are gravitationally unstable. The particles tend to form clumps due to their gravitational attraction, but these clumps are always pulled apart by the shear flow [51, 52]. Thus, the material forms lengthy clumps, called self-gravity or Toomre wakes, with a typical tilt angle of around 20° (relative to azimuthal direction) and a wavelength of around 100 meter [52, 18, 31]. These wakes interfere with other structures which we will discuss later (e.g. generated by the gravity of moons). However, if these induced structures are much larger than the typical wavelength of 100 m, the self-gravity wakes will not alter them directly, but reasonably influence the kinetic transport coefficients. Summarizing, the transport processes in a granular ring particle ensemble are dom! inated by dissipative collisions and the effect of the self-gravity wakes.

3. Hydrodynamic set of equations

The myriad of particles forming the dense rings of Saturn can be modeled as a granular gas, where the motion of the gas is determined due to the gravity of Saturn, its moons and the interactions between the particles. The physics of such a dissipative gas can be described with the help of the hydrodynamic theory.

As already mentioned, planetary rings are very thin discs so that often just vertically integrated values of the rings are observed (as e.g. surface mass density). Thus, it is convenient (if one is not aiming at the vertical structure of the rings) to use vertically averaged quantities to model the rings (mean velocities, granular ring temperature, transport coefficients). For example, the surface mass density can be defined by

$$\Sigma(x, y) = \int_{-\infty}^{+\infty} \rho(x, y, z)\, dz \tag{3.1}$$

by integrating the volume mass density ρ of the ring matter. One can derive a linear relation between surface mass density and the well observable optical depth $\tau \propto \Sigma$ often used for planetary rings (compare with eq. (1.1)).

3.1. Balance equations

The hydrodynamical balance equations (vertically integrated), which describe the motion of the ring particle ensemble, represent three conservation laws: First, the conservation of mass is expressed by the continuity equation

$$\partial_t \Sigma + \nabla \cdot (\Sigma \mathbf{u}) = 0, \tag{3.2}$$

where $\mathbf{u}$ represents the mean velocity. Second, the momentum balance equation gives the evolution of the mean velocity $\mathbf{u}$

$$\Sigma \partial_t \mathbf{u} + \Sigma (\mathbf{u} \cdot \nabla) \mathbf{u} = \mathbf{F} - \nabla \cdot \hat{\mathsf{P}} \, . \tag{3.3}$$

The external and internal volume forces are denoted by $\mathbf{F}$ and $\nabla \cdot \hat{\mathsf{P}}$, respectively. The internal forces are described by the gradient of the pressure tensor $\hat{\mathsf{P}}$. Finally, the conservation of energy (or energy balance equation)

$$\frac{3}{2} \Sigma \left(\partial_t + \mathbf{u} \cdot \nabla \right) T = \nabla \cdot \mathbf{Q} - \hat{\mathsf{P}} : \hat{\mathsf{e}} - \Gamma \tag{3.4}$$

completes the ensemble of hydrodynamic equations. The thermal energy is determined by the trace of the velocity dispersion tensor $T = \mathrm{Tr}\, \hat{\mathsf{P}} / (3\, \Sigma)$, which represents the granular "temperature" of the ring material characterizing the velocity fluctuations. The heat flow in the medium is represented by $\mathbf{Q}$, and $\Gamma(\epsilon)$ measures the loss of heat due to the inelastic collisions. The components of the shear tensor $\hat{\mathsf{e}}$ are defined by

$$e_{ij} = \frac{1}{2} \left(\frac{\partial u_i}{\partial x_j} + \frac{\partial u_j}{\partial x_i} \right) \, . \tag{3.5}$$

3.2. Constitutive Relations

Expressions for the pressure tensor $\hat{\mathsf{P}}$ and the energy flux $\mathbf{Q}$ are needed in order to close the balance equations (3.2)-(3.4). The pressure tensor $\hat{\mathsf{P}}$ can be expressed by Newton's linear constitutive relation

$$\hat{\mathsf{P}} = p \hat{\mathsf{I}} - 2 \Sigma \nu \hat{\mathsf{e}} + \Sigma \left(\frac{2}{3} \nu - \zeta \right) \nabla \cdot \mathbf{u} \, \hat{\mathsf{I}}, \tag{3.6}$$

with the pressure p, the bulk and shear viscosities ζ and ν and the unit tensor $\hat{\mathsf{I}}$. The energy flux $\mathbf{Q}$ can be linearly expressed by Fourier's law

$$\mathbf{Q} = -\kappa \nabla T + \mu \nabla \Sigma \tag{3.7}$$

where κ denotes the heat conductivity. The second term of the energy flux with the coefficient μ arises from the dissipative collisions among the granules and has no analog for molecular gases. Now, the interesting question is, whether and how do the coefficients (p, ν, ζ, κ, μ, Γ) depend on the mean field variables (Σ, $\mathbf{u}$, T)?

3.3. Transport coefficients

Generally, the transport coefficients are functions of the surface mass density Σ and the ring temperature T. However, for granular systems the transport coefficients depend also on the physical conditions of the system – whereas molecular gases are usually not influenced by the physical environment (see discussion section). Important for the rings is the fact that the disc height H scales with the dispersion velocity $c \propto \sqrt{T}$. Thus, the system arranges in a way that the collision frequency ω becomes independent of the velocity dispersion in the first approximation

$$\omega \propto n\,c \propto \frac{\tau}{H}\,H\Omega \propto \Omega\,\tau\,, \tag{3.8}$$

which is the most obvious difference to usual molecular gases.

Unfortunately, the transport coefficients can not be measured directly at Saturn's rings. Thus, several attempts have been made in order to determine these important quantities:

- The coefficients have been calculated theoretically with the help of kinetics [29, 3, 62].
- Numerical N-body simulations have been used in order to calculate the transport coefficients systematically [81, 52, 53, 22].
- The transport coefficients can be additionally estimated by fitting the hydrodynamical models to observed ring structures [26, 77, 70].

The dependencies of the ring viscosity stepped in the focus of ring scientists when examining the stability of dense planetary rings (section 4.1.) as well as their origin and evolution (section 4.2.1.). Several attempts have been made to determine the behavior of the viscosity analytically and numerically.

The kinematic shear viscosity ν connects the shear flow ($\partial u_y/\partial x = -3/2\Omega$ for an unperturbed Kepler disc) and the radial transport of the angular momentum through a plane spanned along the shear flow and vertical direction. The transport of the angular momentum contains three different contributions:

$$\nu = \nu_{\mathrm{l}} + \nu_{\mathrm{nl}} + \nu_{\mathrm{gr}} \tag{3.9}$$

These distinct parts of the shear viscosity arise from different processes: (a) if a particle crosses the reference plane (local, kinematic transport) or (b) if one particle from one side of the reference plane collides with a particle on the other side (non-local transport, arising from finite particle sizes), and (c) if interactions between self-gravity wakes gravitationally amplify the angular momentum transports [22]. Furthermore, massive wakes additionally heat the individual ring particles not belonging to the wake clusters.

The local viscosity ν_{l} can be written as

$$\nu_{\mathrm{l}} = K_1\,\frac{3T}{\Omega}\,\frac{\tau}{1+\tau^2}\,, \tag{3.10}$$

obtained by identifying the pressure tensor component $P_{xy} = P_{r\varphi} = \frac{1}{2}\nu\Omega\Sigma$ (see eq. (3.6)) with the statistically derived expression using the assumption of a triaxial Gaussian velocity distribution

[29]. The nonlocal viscosity component, caused by the finite particle sizes, can be expressed by

$$\nu_{\mathrm{nl}} = K_2\, 4R^2\Omega\tau \tag{3.11}$$

[3, 81, 50, 53]. Both coefficients K_1 and K_2 are of the order of unity. Therefore, the viscosity ν depends on the density Σ and the temperature T of the disc [42, 81]. If self-gravity wakes form in the rings, local and gravitational viscosity can be determined by

$$\nu_{\mathrm{l}} + \nu_{\mathrm{gr}} = K_3 \frac{G^2\Sigma^2}{\Omega^3} \tag{3.12}$$

where ν_{l} and ν_{gr} have equal contributions and K_3 takes values between 2 and 40 depending on the ring region [22]. The scalar local pressure is usually modeled by the gas state equation

$$p = \Sigma\, c^2 \left[1 + \frac{\Omega\, R\tau}{c}\right] , \tag{3.13}$$

where in dense systems the excluded volume due to the finite size of the particles grows in importance. Bulk viscosity ζ and heat conductivity κ are assumed to obey similar dependencies like the shear viscosity [53]. Further, the coefficient μ can be related to the non-local component of the heat conductivity κ as $\mu \propto T\,\kappa_{\mathrm{nl}}/\Sigma$, where μ has to vanish for elastic collisions ($\epsilon \to 1$) [35, 11]. Finally, the granular cooling term is given as

$$\Gamma = K_4\omega(1 - \epsilon^2)\, T\, . \tag{3.14}$$

N-body box simulations have been performed for planetary rings to measure ring temperature and viscosity [42, 81]. Later, this method was used for a complete scan of all hydrodynamic transport coefficients in a non-self-gravitating ring [53] as well as for the investigation of the influence of self-gravity to the velocity dispersion and the viscosity [52, 22].

The transport coefficients can be measured fitting the hydrodynamical models to observed ring structures, but here their dependence on surface density Σ and temperature T have to be guessed beforehand. For example, the damping of the density waves are appropriate to estimate the shear viscosity in a wide range of the A and C ring giving values of 100 and 1 cm^{2}s^{-1}, respectively (e.g. [26, 77]). These values are in a good agreement with the predicted values of N-body simulations [22]. Further, nonlinear effects in strong density waves in Saturn's A ring could be related to a ring pressure $p = \Sigma\, c^2$ with c =3 – 5 mm s^{-1} [70] (see section 4.3.3.).

3.4. Restrictions of the model

Usually, two conditions should be fulfilled in order to apply the hydrodynamic theory to a fluid. First, the mean free path length should be much smaller than the investigated macroscopic structure, and thus, the collision frequency must be much larger than the dynamical frequency ($\approx \Omega$). Second, the mean free path should be much larger than the particle sizes (or the length scale of particle-particle interactions), otherwise correlations between the particles have to be considered additionally.

First the collision frequency is not always large enough, especially considering wavy structures (e.g. moonlet wakes, density waves or overstable waves) which oscillate with the orbital frequency. This raises problems especially for dilute systems, like C ring or Cassini division, where the collision frequency is of the order of the orbital frequency [53]. Thus, there is a delayed reaction of the system to its state and a local thermodynamic equilibrium is not always established. In this case a full kinetic theory would have to be applied to consider this effects. Nevertheless, hydrodynamic models of density waves are also successfully applied to dilute ring regions like Cassini division and C ring [17]. In the denser regions (A and B ring) the collision frequency can increase to around 20 collision per orbit, favoring a hydrodynamical modeling.

The other violation – the mean free path length is of the order of the particle sizes – can be partly accounted using the nonlocal description of the transport coefficients. Nevertheless, the finite correlation length between different ring regions is not regarded in the hydrodynamic description. Even more problematic is the fact that correlations alter the velocity distribution and all related statistic moments – i.e. the state variables. However, the first three statistic moments of the velocity distribution, represented by the hydrodynamical state variables Σ, $\mathbf{u}$, T, will be just sufficient to describe the granular gas if the local velocity distribution is close to a Gaussian equilibrium solution.

4. Applications to planetary rings

As discussed above, the hydrodynamic equations contain some deficits in the physical description of the real ring system. Nevertheless the benefits are still quite impressive, and thus, one finds excellent applications of hydrodynamic modeling in the ring science. Here we will present a few prominent examples:

First, two types of hydrodynamic instabilities which can arise in the unperturbed rings are described. Second, the radial diffusion equation is discussed with its applications to the evolution of the disc and the formation of gaps around embedded moonlets (small moons). Finally, the alternative streamline formalism, using the Newtonian stress relation (3.6), is presented in context of moonlet wakes and density waves.

4.1. Hydrodynamic instabilities in unperturbed rings

In this section perturbations by satellites are neglected and the stability of a homogeneous unperturbed Kepler disc will be discussed characterized by a uniform surface mass density Σ_0, no radial mean velocity $u_0 = 0$ and an azimuthal mean velocity $v_0 = \Omega(r)\, r$ (ground state).

Here a simplified, but illustrative model, is presented in order to analyze the stability of this ground state. The following assumptions are used:

1. An isothermal model is applied.

2. Pressure and self-gravity are neglected.

3. A Cartesian co-rotating frame is used, where $x = r - r_0$ and $y = r_0(\varphi - \varphi_0)$ point to the radial and azimuthal direction, respectively. Curvatures are neglected (Hill approximation).
4. All forces are linearized around the origin ($x = y = 0$) and further the Kepler mean velocity is approximated by the shear stream $v_0 = -3/2\Omega_0\, x$ with $\Omega_0 = \Omega(r_0)$.
5. The hydrodynamic equations (3.2)-(3.3) are linearized around the ground state according to $\Sigma = \Sigma_0 + \sigma$, $u = u'$ and $v = -3/2\,\Omega\, x + v'$, where σ, u' and v' are the deviations from the ground state. Thus, the viscosity can be linearized as $\nu = \nu_0 + \beta\, \nu_0\, \Sigma/\Sigma_0$, where β denotes the gradient of ν with respect to Σ at the ground state.
6. Just radial structures are regarded, and thus, azimuthal dependencies are neglected ($\partial_y \to 0$).

These simplifications lead to the following set of equations:

$$\frac{D\sigma}{Dt} = -\Sigma_0\, \partial_x \cdot u' \tag{4.1}$$

$$\frac{Du'}{Dt} = 2\Omega_0\, v' + \nu_0 \left(\frac{4}{3} + \frac{\zeta}{\nu}\right) \partial_x^2 u' \tag{4.2}$$

$$\frac{Dv'}{Dt} = -\frac{1}{2}\Omega_0\, u' + \nu_0\, \partial_x^2 v' - \frac{3}{2}\Omega_0\, \frac{(1+\beta)\,\nu_0}{\Sigma_0}\, \partial_x \sigma \tag{4.3}$$

where $D/Dt := \partial_t + \mathbf{u} \cdot \nabla$ denotes substantial derivative and the ratio $\frac{\zeta}{\nu}$ is assumed to be constant. Next, a wave solution of the form

$$\begin{pmatrix} \sigma \\ u' \\ v' \end{pmatrix} = \begin{pmatrix} \hat{\sigma} \\ \hat{u}' \\ \hat{v}' \end{pmatrix} \exp(st + ikx) \tag{4.4}$$

is assumed leading to the algebraic system of equations

$$\begin{pmatrix} s & ik\Sigma_0 & 0 \\ 0 & s + k^2\nu_0 \left(\frac{4}{3} + \frac{\zeta}{\nu}\right) & -2\,\Omega_0 \\ ik\frac{3}{2}\Omega_0\, \frac{(1+\beta)\,\nu_0}{\Sigma_0} & \frac{1}{2}\Omega_0 & s + k^2\,\nu_0 \end{pmatrix} \begin{pmatrix} \hat{\sigma} \\ \hat{u}' \\ \hat{v}' \end{pmatrix} = \mathbf{0}\,. \tag{4.5}$$

The system of equations will have a solution if, and only if, the determinant vanishes giving the dispersion relation [56, 65, 55]

$$s^3 + s^2 k^2 \nu_0 \left(\frac{7}{3} + \frac{\zeta}{\nu}\right) + s\left[\Omega_0^2 + k^4 \nu_0^2 \left(\frac{4}{3} + \frac{\zeta}{\nu}\right)\right] + 3\Omega_0^2(1+\beta)\nu_0 k^2 = 0\,. \tag{4.6}$$

This third order polynomial has three solutions which can be expanded for small wavenumbers k aiming at structures with large wavelength. The solutions have possible positive real parts, which lead to unstable modes, being discussed in the next two subsections.

4.1.1. Viscous instability

For small wavenumbers one solution of equation (4.6) reads

$$s_1 = -3\nu_0(1+\beta)k^2 + O(k^3)\,, \tag{4.7}$$

thus, the solution becomes unstable for $\beta < -1$ and the material would flow from diluter to denser regions – small density inhomogeneities are amplified ("up-hill" diffusion) [79, 41].

There has been a long discussion about the existence of viscous instability in the rings in the ring community, especially, in order to explain the observed irregular radial structures found in the Voyager data. The possible existence of a viscous instability stimulated a careful inspection of the dependence of the viscosity ν on the surface mass density Σ [3, 81]. Many of these investigations yielded $\beta > -1$ and viscous instability does not seem to work in dense rings.

4.1.2. Viscous overstability

The other two conjugate complex solutions of equation (4.6) have the form

$$s_{2/3} = \pm i\Omega_0 + \frac{3}{2}\nu_0 k^2 \left[\beta - \frac{1}{3}\left(\frac{\zeta}{\nu} - \frac{2}{3}\right)\right] + O(k^3) \tag{4.8}$$

allowing oscillations to evolve. The disc will become unstable if the gradient β becomes larger than a critical value

$$\beta > \beta_{\text{crit}} = \frac{1}{3}\left(\frac{\zeta}{\nu} - \frac{2}{3}\right). \tag{4.9}$$

In this case an oscillatory instability appears – called viscous overstability.

The possible occurrence of overstability in the rings was first recognized on base of a streamline model [8]. Later a systematic linear analysis of the hydrodynamic equations, including the effect of pressure and self-gravity, was presented [56]. This model has been further developed including the effect of thermal diffusion and better estimates of the transport coefficients [65, 55]. The appearance of overstability could be demonstrated in N-body simulations of the rings which partly can coexist with self-gravity wakes [53]. In recent studies the nonlinear effects [54, 38, 39] and a more general kinetic analysis [36, 37] have been included which has improved the overstability model.

Radial wavelike axisymmetric structures with a wavelength of 100 - 200 m have indeed been found independently in UVIS and RSS occultation scans of Cassini [19, 74], proving the existence of overstability in the rings.

4.2. Diffusion in the rings

The interactions between the particles can not only cause instabilities they can also cause a diffusion of ring particles smoothing out inhomogeneities in the ring density Σ. The generation of these inhomogeneities can be of different origin – we will focus on gravitational perturbations by embedded moons. Most of the ring structures are stretched in azimuthal direction, so that the radial diffusion of the ring material is of main interest.

The radial mean velocity u_r is much smaller than the azimuthal velocity $r\Omega$, which is almost not influenced by the diffusion. With these assumptions the mean azimuthal velocity component can be considered to be stationary and is written in polar coordinates as [45, 48, 73]

$$r\Sigma u_r = -3\sqrt{r}\partial_r(\sqrt{r}\nu\Sigma) \tag{4.10}$$

assuming that the diffusion of the particles is mainly caused by the Kepler shear. Combining this equation with the continuity equation (polar coordinates) one obtains a non-linear diffusion equation for the dense rings

$$\partial_t\Sigma + (\Omega - \Omega_0)\partial_\varphi\Sigma = \frac{3}{r}\partial_r\left[\sqrt{r}\partial_r(\sqrt{r}\nu\Sigma)\right] \tag{4.11}$$

where a co-rotating frame has been chosen fixed at (a_0,$\Omega_0 t$).

4.2.1. Evolution of the ring

The diffusion equation is related to a characteristic time scale

$$t_{\text{diff}} = \frac{(\Delta r)^2}{\nu}. \tag{4.12}$$

One possible ring origin scenario assumes that the rings have been formed in a catastrophic disruption of a parent body (e.g. moon, comet). A spreading of the fragments to the present dense ring width of $\Delta r \approx 44,000$ km (A and B ring) would need $t_{\text{diff}} \approx 5 \cdot 10^9$ yr assuming $\nu = 100$ cm^2 s^{-1}, which is about the age of our Solar system. However, the time scale is sensitive to the viscosity, and thus also to the surface mass density, which was much higher in the ancient rings. Moreover, the surface mass density is still not well known for the B ring. Therefore, the measurement of the ring mass became one of the major goals of the Cassini mission. More precise models, which have been published recently [16, 49], confirmed the age of the rings to be between $3 \cdot 10^9$ and $4 \cdot 10^9$ years. Furthermore, it has been shown that resonances with moons vividly influence the diffusion of the ring material! . These resonances force the production of moons with a certain size at the outer A ring edge [16].

4.2.2. Gaps induced by embedded moonlets

Moons embedded in the rings perturb the surrounding particle ensemble due to their gravity, resulting in the formation of structures around the moon which can serve as "fingerprints" for their detection. The diffusion is counteracting the structure formation, which leads to a smoothing out of the induced structures. Spahn and Sremčević developed a model of the balance of probabilistic scattering and viscous diffusion in order to combine both competing effects [68]. The model makes use of the fact that the zone of gravitational influence of the moon is rather small in comparison to the azimuthal extent of the induced structures. This length of gravitational influence is related to the Hill radius

$$h = a_{\mathrm{m}} \left(\frac{M_{\mathrm{m}}}{3M_{\mathrm{s}}} \right)^{1/3} , \tag{4.13}$$

which depends on the mass of the moon M_{m}, the mass of Saturn M_{s} and the semi-major axis of the moon a_{m}.

Neglecting the particle interactions one can perform test particle integrations of the equation of motion [63, 69]. Three types of particle behavior and related structures can be distinguished, depending on the radial distance $x = r - a_{\mathrm{m}}$ in which the particles enter the moon:

1. Particles with small impact parameter $|x| = |r - a_{0,\mathrm{in}}| < 1\,h$ move on horseshoe orbits. They slowly approach the moon and meanwhile exchange energy leading to a flipping of the impact parameter $x_{\mathrm{out}} \approx -x_{\mathrm{in}}$. The eccentricity remains almost unchanged but varies significantly for $x_{\mathrm{in}} \to 1h$ [25, 24, 69, 67].

2. Particles with impact parameter in the range $1h < |x_{\mathrm{in}}| < 4h$ are heavily scattered by the moon. Partly, the particles move on chaotic orbits and the final radial mean positions x_{out} change drastically. This causes a depleted region of material at this radial position (gap) [33, 43, 46, 69, 67].

3. The semi-major axis almost does not change during an encounter for particles with large initial impact parameter $|x_{\mathrm{in}}| > 4h$ but the moonlet induces a systematic eccentricity $\propto x^{-2}$ resulting in a wavy like density structure in this region, called moonlet wakes [21, 60, 10, 66, 34, 40].

The diffusion of the particles causes the density depleted regions (gaps), formed by the moon, to smooth out along the azimuth. This diffusion can be modeled by the equation (4.11) if one uses the moon produced radial density distribution $\Sigma(r, \phi = 0)$, gained from test particle integrations, as a boundary condition [68]. Figure 2 shows the resulting radial density profile after a single scattering. The complete stationary density signature after many single scatterings is presented in figure 3. The moonlet wakes are not visible in this model, because systematic and coherent particle motions have been averaged out [68]. Two qualitative different structures can be distinguished based on the sizes of the moons: (a) a S-shaped density structure - called propeller - for small moons with radii $R_{\mathrm{moon}} < 500$ m which are just local density perturbations and (b) a completely open! ed and empty gap produced by a moon with radius $R_{\mathrm{moon}} > 500$ m [68].

Both types of structures have indeed been observed in Voyager and Cassini spacecraft data. Saturn's rings habit two known larger moons named Pan and Daphnis [59, 47] orbiting in empty gaps being swept free by their gravity. To date, more than 150 propeller structures have meanwhile been detected in the images of the Cassini cameras pointing to smaller moons with radii of around 50 meter up to a few hundred meters in the A ring [76, 71, 75, 78].

An analytical solution for the model using a linearized version of the diffusion equation (4.11)

$$\frac{\Omega_0}{2\,(1+\beta)\,\nu_0} \partial_y \sigma = -\frac{1}{x} \partial_x^2 \sigma \tag{4.14}$$

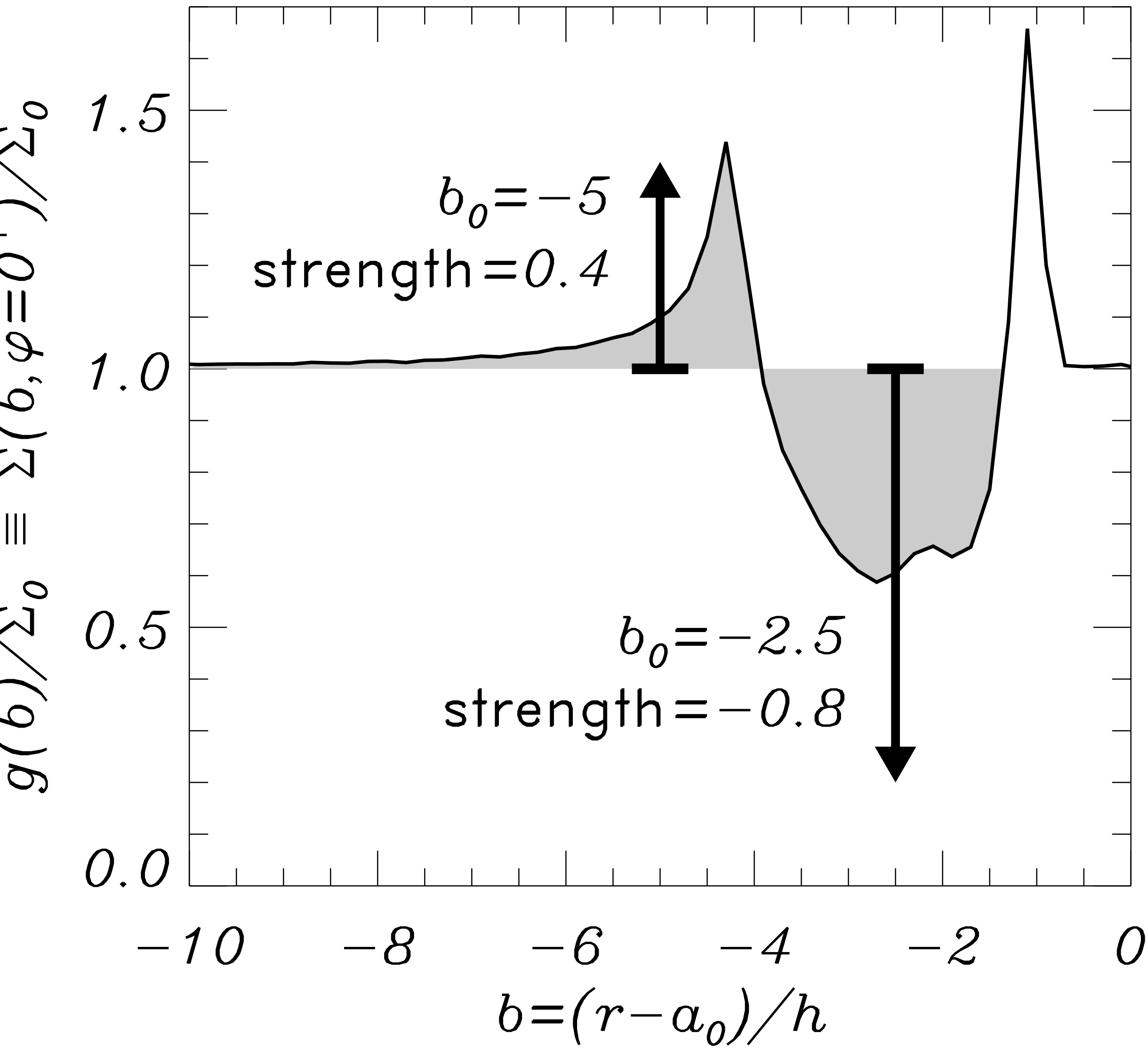

Figure 2: The density profile is shown after the gravitational scattering due to the moon. A density depleted region at around 2 h is visible with two adjacent regions of enhanced material. The arrows indicate the strength and mean point of the perturbations as used for equation (4.17) (figure taken from ref. [72]).

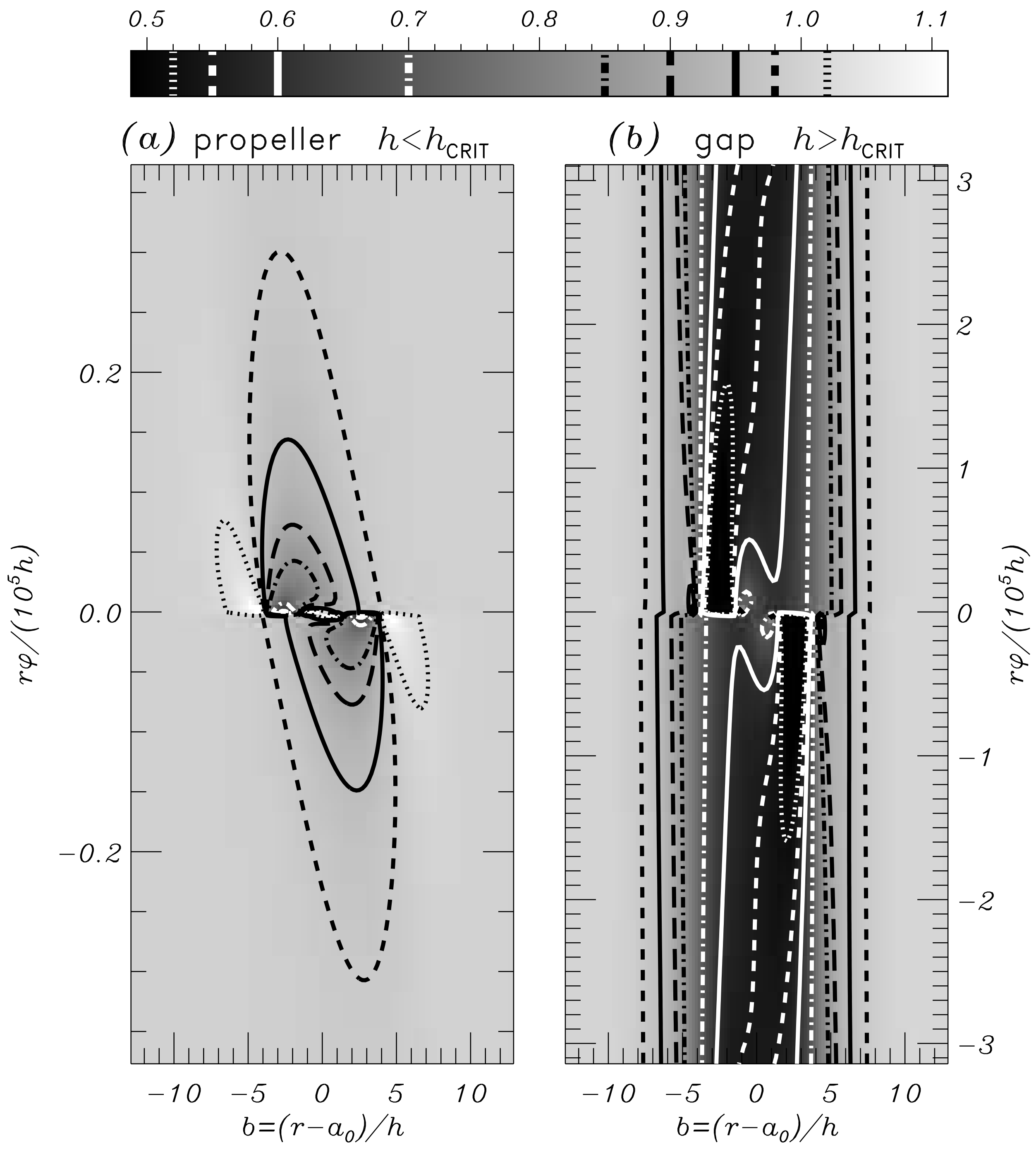

Figure 3: Two numerical solutions of equation (4.11) are presented for different moon sizes. The small moon is just producing a local S-shaped structure of two radial separated gaps, whereas the large moon produces a complete empty gap going around the whole circumference of the ring (figure taken from ref. [72]).

could be derived [72] where the definitions of the linearized quantities are analog to those given in section 4.1.

The radial structure of the moonlet density profile can be scaled with the Hill radius h of the moonlet. Thus, if one applies this scaling law to the linear diffusion equation (4.14) with $\tilde{x} = x/h$, one can also conclude a scaling law for the azimuthal direction as [68, 72]

$$a_0 K = \frac{\Omega_0\, h^3}{2(1+\beta)\nu_0} \propto \frac{M_{\mathrm{moon}}}{\nu_0}\,. \tag{4.15}$$

and a scaled azimuthal coordinate can be defined as $\Phi = y/(a_0 K)$. Thus, inferring the moonlet mass from the radial structure, the viscosity of the ring can be gained from the azimuthal extent of the gaps [68]. These scaling laws could be confirmed by N-body simulations [58].

An approximate Green solution solving the problem for $\sigma = \delta(\tilde{x} - \tilde{x}_0)$ has been found [72] in the form

$$G(\tilde{x}, \Phi, \tilde{x}_0) = -\frac{\sqrt{3}\tilde{x}_0}{2}\,(3\Phi)^{-2/3} \exp\left[\frac{\tilde{x}^3 + \tilde{x}_0^3}{9\Phi}\right] \mathrm{Bi}\left[(3\Phi)^{-2/3}\,\tilde{x}_0\tilde{x}\right]\,, \tag{4.16}$$

and it has been shown that the source function of the density depletion can be approximated by a combination of 3 weighted $\delta(\tilde{x} - \tilde{x}_0)$ functions. Thus, the solution of the density perturbation can be written as

$$\frac{\Sigma(\tilde{x}, \Phi)}{\Sigma_0} = 1 + 0.16\, G(\tilde{x}, \Phi, -1) - 0.76\, G(\tilde{x}, \Phi, -2.5) + 0.26\, G(\tilde{x}, \Phi, -5)\,. \tag{4.17}$$

Figure 4 (upper part) shows the density distribution around a moon with 20 meter radius, using the analytical solution (4.17). This structure has additionally been superposed by a wave-like wake pattern obtained by an analytic model presented in section 4.3.2.. The lower panel of figure 4 shows the result of a N-body simulation for comparison [58]. The analytical solution deviates from the simulation close to the azimuthal position of the moon, because of two model assumptions: (a) The moon gravity action is reduced to the position $y = \Phi = 0$ (scattering line) and (b) the initial density distribution is approximated by three weighted δ-functions. However, the density distribution of the analytical solution and the simulation converge to each other for growing azimuth resulting in a fair agreement [58] between analytics and numerics.

Many S-shaped "propeller" structures (> 150) have already been observed in the Cassini imaging data [76, 71, 75, 78]. Difficulties arise in the interpretation of the images, because one cannot deduce the density in the rings from the observed brightness directly. Thus, photometric modeling of the observed structure is needed to get a better interpretation [71]. The mass and the radii of the moons, producing the observed "propellers", could be estimated on the base of radial predicted structures [68, 72, 58], which led to inferred moonlet radii between 50 - 500 meter. Thus, there exists an additional moonlet population having sizes much larger than those of the main ring particle population ranging from several centimeters to tens of meters. The moonlet size distribution follows a rather steep power law with indices between -5 and -10 in ! contrast to the main particle size distribution with an index of around -3 [71, 75]. Difficulties still exist in the interpretation of the azimuthal gap length to quantify the ring viscosity offering opportunities for future studies.

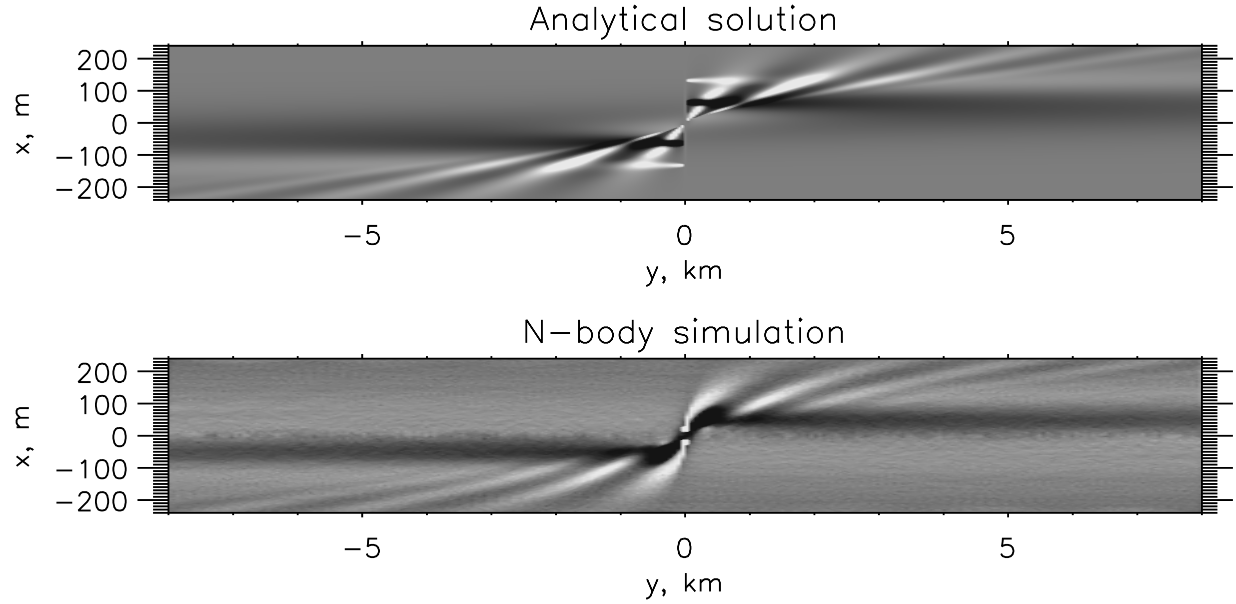

Figure 4: Density distribution of a propeller induced by a moon with radius of 20 m. The analytical propeller model is plotted in the upper panel combining the gap (eq. (4.17)) and wake model (see section 4.3.2.). The result of a N-body simulation is shown for comparison in the lower panel.

4.3. Streamline formalism

The following concept is ideally suited to describe perturbed regions of dense planetary rings, especially if oscillatory structures are studied caused by the systematic excitation of the particle eccentricities (e.g. moonlet induced wakes or density waves). Unperturbed particles move on Kepler ellipses around Saturn oscillating around its radial mean position. Therefore, it is convenient to use this knowledge about the solution and look how interactions between the particles change their orbits. Based on this idea, Borderies, Goldreich and Tremain introduced the streamline formalism to planetary rings in the 1980'ties. The idea is to follow particles along their streamline and to calculate perturbations on the particles arising from certain interactions [5].

The streamline positions and velocities can be written in the form [6, 5, 57]

$$
\begin{aligned}
x &= X - ea_0 \cos\phi && (4.18)\\
y &= Y + 2ea_0 \sin\phi && (4.19)\\
u &= ea_0\Omega_0 \sin\phi && (4.20)\\
v &= -\frac{3}{2}\Omega_0 X + 2ea_0\Omega_0 \cos\phi, && (4.21)
\end{aligned}
$$

with the angle $\phi = \Omega_0 t - \varpi$ and $Y = -3/2\, X\Omega_0 t$ (set $y_0 = 0$). The eccentricity of the particle in the streamline and its reduced semi-major axis are denoted by e and $X = a - a_0$, respectively. The distance between the streamlines changes due to the perturbations leading to a compression or decompression of the material in this regions quantified by

$$J = \frac{dx}{dX} = 1 - a_0 \frac{de}{dX} \cos\phi + e a_0 \frac{d\phi}{dX} \sin\phi \tag{4.22}$$

$$= 1 + q\cos(\phi + \gamma'), \tag{4.23}$$

where the term $d\phi/dX$ is identified with the radial wave number k. The non-linearity parameter and the phase shift are labeled by q and γ', respectively, and are defined by

$$q\cos\gamma' = -a_0 \frac{de}{dX} \tag{4.24}$$

$$q\sin\gamma' = -a_0 e \frac{d\phi}{dX} \,. \tag{4.25}$$

Thus, the surface mass density is obtained by

$$\Sigma = \frac{\Sigma_0}{J} \,, \tag{4.26}$$

using the compression factor J^{-1}.

Usually structures in planetary rings get very elongated in azimuthal direction because of the Kepler shear which stretches all structures in this direction. Thus, radial changes for density and mean velocities dominate over azimuthal changes (tight winding approximation) and the radial gradient of the eccentricity becomes much smaller than the radial gradient of the phase ϕ in the tight winding approximation. Therefore, we will use the approximations $q \approx a_0 e \cdot |k|$ and $\gamma' \approx -\pi/2\,\mathrm{sign}(X)$ in the following.

The perturbations are assumed to lead to small changes of eccentricity e and longitude of pericenter ϖ during one orbital period. Thus, their time evolution can be calculated by means of the orbit averaged Gaussian perturbation equations

$$\frac{de}{dt} = \frac{1}{2\pi\, a_0 \Omega_0} \int_0^{2\pi} \left(G_x \sin\phi + 2G_y \cos\phi\right)\, d\phi \tag{4.27}$$

$$\frac{d\varpi}{dt} = \frac{1}{2\pi\, e\, a_0 \Omega_0} \int_0^{2\pi} \left(-G_x \cos\phi + 2G_y \sin\phi\right)\, d\phi \tag{4.28}$$

which are given in a linearized form for small eccentricities $e \ll 1$ and $\mathbf{G} = (G_x, G_y)$ denotes the acceleration at the streamline.

4.3.1. Effect of Newtonian stress

The collisions between the ring particles lead to an acceleration $\mathbf{G}$ of the particles which is modeled by the gradient of the pressure tensor $\hat{\mathsf{P}}$

$$\mathbf{G} = -\frac{1}{\Sigma} \nabla \cdot \hat{\mathsf{P}} \,. \tag{4.29}$$

Considering the structures being tightly wound, the calculation of the radial and azimuthal accelerations reduces to

$$G_x = -\frac{1}{\Sigma}\frac{dP_{xx}}{dx} = -\frac{k}{\Sigma_0}\frac{dP_{xx}}{d\phi} \tag{4.30}$$
$$G_y = -\frac{1}{\Sigma}\frac{dP_{xy}}{dx} = -\frac{k}{\Sigma_0}\frac{dP_{xy}}{d\phi}. \tag{4.31}$$

with $d/dx = J^{-1}\, d/dX = k\, J^{-1}\, d/d\phi$. If one combines the equations (4.27)-(4.28) with the equations (4.30)-(4.31) and integrates them by parts one will obtain

$$\frac{de}{dt} = \frac{k}{2\pi\,\Sigma_0\, a_0\Omega_0}\int_0^{2\pi}(P_{xx}\cos\phi - 2P_{xy}\sin\phi\,)\,d\phi \tag{4.32}$$
$$\frac{d\varpi}{dt} = \frac{k}{2\pi\,\Sigma_0\, e\, a_0\Omega_0}\int_0^{2\pi}(P_{xx}\sin\phi + 2P_{xy}\cos\phi\,)\,d\phi\,, \tag{4.33}$$

and for the radial derivatives of the velocities one may write

$$\frac{du}{dx} = J^{-1}\frac{du}{dX} = J^{-1}q\Omega_0\cos(\phi) \tag{4.34}$$
$$\frac{dv}{dx} = J^{-1}\frac{dv}{dX} = J^{-1}\Omega_0(-\frac{3}{2} - 2q\sin(\phi)). \tag{4.35}$$

Now the components of the pressure tensor can be calculated using the relation (3.6). If we assume an isothermal model with scalar pressure $p = \Sigma\, c^2$ (ideal gas) and transport coefficients as used in section 4.1. the pressure tensor can be written in the form

$$P_{xx} = c^2\Sigma_0\frac{1}{J} - \nu_0\Sigma_0\Omega_0\left(\frac{4}{3}+\frac{\zeta}{\nu}\right)\frac{\cos\phi}{J^{2+\beta}} \tag{4.36}$$
$$P_{xy} = \nu_0\Sigma_0\Omega_0\left(\frac{3}{2}+2q\sin\phi\right)\frac{1}{J^{2+\beta}}. \tag{4.37}$$

Finally, the perturbation equations can be written in the form

$$\frac{de}{dt} = -\frac{\nu_0 k}{a_0}f(q,\beta,\frac{\zeta}{\nu}) \tag{4.38}$$
$$\frac{d\varpi}{dt} = -\Omega_0 c^2 k^2 g(q)\,. \tag{4.39}$$

Equation (4.38) describes the viscous damping of the eccentricity e, whereas the pressure force, which does not dissipate energy, mainly changes the longitude of pericenter ϖ and thus the wavelength of the oscillatory structure. General Solutions for $f(q,\beta,\frac{\zeta}{\nu})$ and $g(q)$ are given in ref. [57].

The nonlinearity parameter q can come close to unity where the functions $f(q,\beta,\frac{\zeta}{\nu})$ and $g(q)$ become highly nonlinear, for instance, in case of wakes induced by the large embedded moons or at strong resonances. Here, we will concentrate on small perturbations where the nonlinearity parameter q stays small for simplicity. Then the solutions reduce to

$$f(q \to 0, \beta, \frac{\zeta}{\nu}) = -\frac{3}{2}(\beta - \beta_{\text{crit}})\, q \tag{4.40}$$

$$g(q \to 0) = \frac{1}{2}. \tag{4.41}$$

where the definition of β_{crit} is adapted from equation (4.9). Thus, we rediscovered the condition for viscous instability in the streamline formalism and $\beta < \beta_{\text{crit}}$ is regarded for the damping of the eccentricity [8].

4.3.2. Applications to moonlet induced wakes

In section 4.2.2. it has already been discussed that particles, which pass the perturbing moon distant enough, are just slightly deflected. Their semi-major axis is not changing significantly, but they get an induced eccentricity $e_0 = C\, h^3/(a_0 x^2)$ with $C = 6.72$ and a synchronous and coherent phase $\varpi_0 = \pi/2\, \text{sign}(x)$. This synchronous phase together with the Kepler shear produces a wavy like pattern at the edges - called moonlet wakes [60], which should not be confused with the self-gravity wakes!

In case of moon wakes the relation

$$\phi = -\frac{2Y}{3X} - \varpi \tag{4.42}$$

can be derived from the definitions of ϕ and Y [60]. Thus the radial wavenumber $k = d\phi/dX = 2Y/(3X^2) = -\Omega_0 t/X$ becomes time dependent and the wakes wind up along the azimuth. The radial gradient of the eccentricity $de/dX \approx -2\, e/X$ is much smaller than the radial gradient of the phase ϕ which justifies the tight winding approximation.

Thus, the differential equation (4.38) can be solved using equation (4.40) to give for the eccentricity

$$e(t) = e(0) \exp\left\{ \frac{\nu_0}{2X^2}(\beta - \beta_{\text{crit}})\, \Omega_0^2 t^3 \right\}. \tag{4.43}$$

Therewith, the linearized solution for the nonlinearity parameter q becomes

$$q(t) = a_0 e(0) \frac{\Omega_0 t}{X} \text{sign}(X) \exp\left\{ \frac{\nu_0}{2X^2}(\beta - \beta_{\text{crit}})\, \Omega_0^2 t^3 \right\}. \tag{4.44}$$

This analytical solution has been plotted in figure 4 together with the propeller gap model (see section 4.2.2.). The wakes are in good agreement with the numerical solution. The wake crest amplitude appeared just too strong for small radial distances and thus the nonlinearity parameter q had to be restricted below 1. This restriction could be lifted using the full nonlinear expressions of $f(q \to 0, \beta, \frac{\zeta}{\nu})$ and $g(q)$ [10, 57].

The most important restriction of this model is the assumption of a constant granular temperature in the wakes. However, the qualitative damping behavior of the wakes is not affected by this simplifications [10, 40]. The change of the granular temperature in the non-isothermal case would mainly lead to an increase of the mean viscosity and thus to a more efficient wake damping.

4.3.3. Applications to density waves

Moons also induce large eccentricities to the ring particles over large radial distances if their orbital motion is in resonance with a certain ring region where the particles get a periodic kick (commensurable with their orbital frequency). An important form is the Lindbland resonance defined by the condition

$$(m-1)\,\Omega_0 = m\,\Omega_f \tag{4.45}$$

where Ω_0 is the orbital frequency of the resonance position and Ω_f denotes the pattern speed of the induced perturbation, which can be related to the orbital motion of the moon. Inner and outer Lindbland resonances occur for the integer $m > 0$ and $m < 0$, respectively, where m denotes the order of the resonance. The excitation of the particles at resonances can generate waves in the ring density as a result of an interplay between gravitational stress (Maxwell stress-tensor of gravity) and inertia forces (Coriolis) which widely occur in Saturn's rings [28, 61, 9]. Their observation permits to quantify the surface mass density and the viscosity in the rings. The surface mass density can be gained from the data using the wave dispersion relation, which shall be derived here on base of the streamline formalism.

The streamlines go around Saturn and have to be closed. Thus, the phase $\phi = \Omega(r)t - \varpi$ must satisfy the condition $\phi = m(\Omega(r) - \Omega_{\mathrm{f}})t$, thus

$$\frac{d\varpi}{dt} = \Omega(r) - m(\Omega(r) - \Omega_{\mathrm{f}}). \tag{4.46}$$

Now, $\Omega(r)$ can be linearized around the resonance location as $\Omega(r) \approx \Omega_0 - 3\Omega_0\, x/(2a_0)$ and Ω_{f} can be replaced by equation (4.45), resulting in

$$\frac{d\varpi}{dt} = \frac{3\Omega_0}{2a_0}(m-1)\,x\,. \tag{4.47}$$

The precession of ϖ is caused by particle interactions, where the contribution of self-gravity can be calculated in a similar way as the effect of Newtonian stress and the change in the pericenter position reads [9]

$$\frac{d\varpi}{dt} = \frac{\pi G \Sigma_0}{\Omega_0}|k|h(q). \tag{4.48}$$

A general expression of $h(q)$ is given for example by ref. [9], where the function fulfills $h(q) \to 1$ for $q \to 0$.

Combing the radial dependence of the precession (4.47) with the contributions of the particle interactions given by the equations (4.39) and (4.48) results in the dispersion relation:

$$\frac{3\Omega_0}{2a_0}(m-1)\,x = \frac{\pi G \Sigma_0}{\Omega_0}|k| - \frac{c^2}{2}k^2 \tag{4.49}$$

Figure 5 shows the Janus 2:1 density wave in a PPS optical depth profile together with a wavelet power spectrum as an example. The dispersion relation (4.49) has been fitted to the spectrum giving a surface mass density of 700 kg m^{-2}, whereas the smaller nonlinear contribution due to the pressure gradient has been neglected (second term in eq. (4.49)).

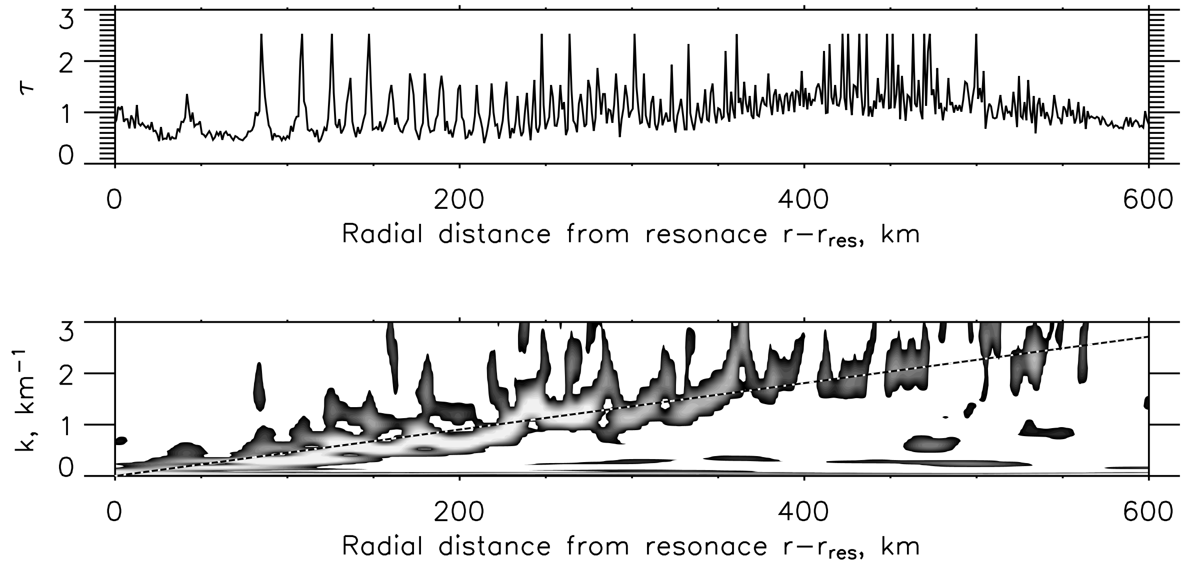

Figure 5: Upper Panel: Optical depth profile of the Janus 2:1 Lindblad resonance in Saturn's B ring from the Voyager PPS scan. Lower Panel: Wavelet spectrum from the profile above. A clear trend in the wavenumber k is visible, which can be explained by the dispersion relation (4.49) if a surface mass density of $\Sigma = 700$ kg m^{-2} is assumed.

5. Discussion

Planetary rings are – apart from their beauty and wealth of structures – the only real examples of granular gases in nature. The quantitative description of their physical nature using macroscopic or mean field balances of dense granular flows has been a challenge for decades.

Kinetic theory appears to be the most appropriate approach to explain the behavior of the granular shear flow in Saturn's rings. However, the mathematical treatment is quite difficult for most applications. While kinetics of dissipatively colliding ring particles are useful to describe the steady state of the rings – characterized by viscous heating and collisional dissipative cooling – perturbed regions and related structures can easier be characterized by mean field balances of mass, momentum and energy: a reduction of the kinetic description to hydrodynamic moments.

The problem, however, is that the properties of granular gases, transports and equation of state, are not universal for granular gases and rather depend on the physical conditions. The physical reason is found in a lack of a scale separation between size of the ring particles (interaction length scale), the mean free path between them and the spatial scale on which mean field quantities (density, mean velocities and temperature) may change. For instance the molecular interaction scale for molecular gases is in the order of the size of the molecules (Angstroms), their mean free path is in the order of micrometers (depending on pressure and density), and densities, mean velocities and temperatures of the flow usually change on scales larger than centimeters (depending on the system investigated). In other words, these scales are separated by many orders of magnitudes for "normal" gases or fluids, whereas they are of the same order for dense granular gases like in Saturn's ring! s.

This lack of scale separation is the reason that the transports have to be quantified separately for each physical situation the granular gas rests in. The latter means, for instance, gradients of external forces, which may show spatial scales in the order of the sizes of the granules and of their mean free path. Thus, gradients of forces and of the state variables change over the mean free path – indirectly influencing the matter properties of the granular gas.

Therefore the observed features (overstability or propellers) found in the A ring might not be expected to evolve in other ring regions, like the much denser B ring or the less denser C ring. It could well be that there a moonlet may not be able to generate an observable propeller or that overstable waves do not emerge, although the condition for the instability is formally fulfilled. One reason could be that a linear Newton constitutive relation is not sufficient anymore to describe the transports in the rings and non-linear relations would be needed. Thus, the critical problem of the reduced hydrodynamical approach is the characterization of the transports (closure of balance equations): The relation between shear and momentum transfer as well as between gradients of the velocity dispersion (temperature) and heat flow mediated by the viscosities ν and ζ, the heat conductivity κ and the coefficient μ, respectively. In this sense we have to state that th! e hydrodynamical description is not of general use for all granular flows.

Nevertheless, we demonstrated the benefit of the hydrodynamical approach in this review using the structural examples of overstability, moonlet induced propeller-features, and density waves at resonance locations – which are all structures that have been predicted theoretically and later detected by experiments of the space vehicles Voyager and Cassini.

In the case of viscous overstability the linear ansatzes and proper parameterizations of the transports have been sufficient to predict the overstable viscous waves [65, 55, 53] obeying properties which have indeed been confirmed by the Cassini experiments [19, 74]. These observations seem to support the Fourier and Newton constitutive relations for the energy and momentum transports, respectively, and the hydrodynamic approach in general, further allowing to estimate granular viscosities in the rings. Also the more general investigation of the overstable waves using kinetic theory could confirm the predictions due to the hydrodynamic approach [36, 37].

The prediction of the propeller-structures [68, 72, 58] caused by embedded skyscraper-sized moonlets supports the hydrodynamics in perturbed ring regions as well. Meanwhile more than one hundred propellers have been observed in the outer A ring of Saturn and even a few of the largest of them show all features predicted by theory [76, 71, 75, 78]. However, careful inspections of the observed propeller yielded that the particle size distribution is changing in the perturbed regions – not included in the hydrodynamic model – which is substantial for the interpretation of the observations [71] and could also have influence on the transport of momentum and heat.

These successes motivate to model structures in planetary rings using the hydrodynamical approach also in future even if kinetic theory offers a more accurate description of the rings. A development of a simulation code, as used for preplanetary discs, would also be a worthwhile goal in order to investigate ring structures.

Acknowledgements

We are grateful to the referee reviewing this article. This work was supported by Deutsche Forschungsgemeinschaft (Sp 384/25-1).

References

[1] N. Albers, F. Spahn. *The influence of particle adhesion on the stability of agglomerates in Saturn's rings*. Icarus, 181 (2006), 292–301.

[2] J. P. Andrews. *Theory of Collision of Spheres of Soft Metals*. Phil.Mag.S.7, 9 (1930), 58, 593–610.

[3] S. Araki, S. Tremaine. *The dynamics of dense particle disks*. Icarus, 65 (1986), 83–109.

[4] J. M. Barbara, L. W. Esposito. *Moonlet Collisions and the Effects of Tidally Modified Accretion in Saturn's F Ring*. Icarus, 160 (2002), 1, 161–171.

[5] N. Borderies. *Ring dynamics*. Celestial Mechanics and Dynamical Astronomy, 46 (1989), 207–230.

[6] N. Borderies, P. Goldreich, S. Tremaine. *Sharp edges of planetary rings*. Nature, 299 (1982), 209–211.

[7] N. Borderies, P. Goldreich, S. Tremaine. *Unsolved problems in planetary ring dynamics*. In Planetary Rings (1984) pages 713–734.

[8] N. Borderies, P. Goldreich, S. Tremaine. *A granular flow model for dense planetary rings*. Icarus, 63 (1985), 406–420.

[9] N. Borderies, P. Goldreich, S. Tremaine. *Nonlinear density waves in planetary rings*. Icarus, 68 (1986), 522–533.

[10] N. Borderies, P. Goldreich, S. Tremaine. *The formation of sharp edges in planetary rings by nearby satellites*. Icarus, 80 (1989), 344–360.

[11] J. J. Brey, J. W. Dufty, C. S. Kim, A. Santos. *Hydrodynamics for granular flow at low density*. Physical Review E, 58 (1998), 4638–4653.

[12] F. G. Bridges, A. Hatzes, D. N. C. Lin. *Structure, stability and evolution of Saturn's rings*. Nature, 309 (1984), 333–335.

[13] N. Brilliantov, F. Spahn, J.-M. Hertzsch, T. Pöschel. *Model for collisions in granular gases*. Physical Review E, 53 (1996), 5382–5392.

[14] N. V. Brilliantov, N. Albers, F. Spahn, T. Pöschel. *Collision dynamics of granular particles with adhesion*. Phys. Rev. E, 76 (2008), 051302.

[15] R. M. Canup, L. W. Esposito. *Accretion in the Roche zone: Coexistence of rings and ring moons.* Icarus, 113 (1995), 331–352.

[16] S. Charnoz, J. Salmon, A. Crida. *The recent formation of Saturn's moonlets from viscous spreading of the main rings*. Nature, 465 (2010), 752–754.

[17] J. E. Colwell, J. H. Cooney, L. W. Esposito, M. Sremčević. *Density waves in Cassini UVIS stellar occultations. 1. The Cassini Division*. Icarus, 200 (2009), 574–580.

[18] J. E. Colwell, L. W. Esposito, M. Sremčević. *Self-gravity wakes in Saturn's A ring measured by stellar occultations from Cassini*. Geophysical Research Letters, 33 (2006), 7201.

[19] J. E. Colwell, L. W. Esposito, M. Sremčević, G. R. Stewart, W. E. McClintock. *Self-gravity wakes and radial structure of Saturn's B ring*. Icarus, 190 (2007), 127–144.

[20] J. N. Cuzzi, J. J. Lissauer, L. W. Esposito, J. B. Holberg, E. A. Marouf, G. L. Tyler, A. Boischot. *Saturn's Rings: Properties and Processes*. In Planetary rings (R. Greenberg, A. Brahic, editors), pages 73–199, The University of Arizona Press 1984.

[21] J. N. Cuzzi, J. D. Scargle. *Wavy edges suggest moonlet in Encke's gap*. Astrophysical Journal, 292 (1985), 276–290.

[22] H. Daisaka, H. Tanaka, S. Ida. *Viscosity in a Dense Planetary Ring with Self-Gravitating Particles*. Icarus, 154 (2001), 296–312.

[23] D. R. Davis, S. J. Weidenschilling, C. R. Chapman, R. Greenberg. *Saturn ring particles as dynamic ephemeral bodies*. Science, 224 (1984), 744–747.

[24] S. F. Dermott, C. D. Murray. *The dynamics of tadpole and horseshoe orbits. I - Theory. II - The coorbital satellites of Saturn*. Icarus, 48 (1981), 1–22.

[25] S. F. Dermott, C. D. Murray, A. T. Sinclair. *The narrow rings of Jupiter, Saturn and Uranus*. Nature, 284 (1980), 309–313.

[26] L. W. Esposito, M. Ocallaghan, R. A. West. *The structure of Saturn's rings - Implications from the Voyager stellar occultation*. Icarus, 56 (1983), 439–452.

[27] R. G. French, P. D. Nicholson. *Saturn's Rings II. Particle sizes inferred from stellar occultation data*. Icarus, 145 (2000), 502–523.

[28] P. Goldreich, S. Tremaine. *The excitation and evolution of density waves*. Astrophysical Journal, 222 (1978), 850–858.

[29] P. Goldreich, S. D. Tremaine. *The velocity dispersion in Saturn's rings*. Icarus, 34 (1978), 227–239.

[30] A. Hatzes, F. G. Bridges, D. N. C. Lin. *Collisional properties of ice spheres at low impact velocities*. Mon. Not. R. Astr. Soc., 231 (1988), 1091–1115.

[31] M. M. Hedman, P. D. Nicholson, H. Salo, B. D. Wallis, B. J. Buratti, K. H. Baines, R. H. Brown, R. N. Clark. *Self-Gravity Wake Structures in Saturn's A Ring Revealed by Cassini VIMS*. Astronomical Journal, 133 (2007), 2624–2629.

[32] D. Heißelmann, J. Blum, H. J. Fraser, K. Wolling. *Microgravity experiments on the collisional behavior of saturnian ring particles*. Icarus, 206 (2010), 424–430.

[33] M. Henon. *A simple model of Saturn's rings*. Nature, 293 (1981), 33–35.

[34] J.-M. Hertzsch, H. Scholl, F. Spahn, I. Katzorke. *Simulation of collisions in planetary rings.* Astronomy and Astrophysics, 320 (1997), 319–324.

[35] J. Jenkins, M. Richman. *Grad's 13-moment system for a dense gas of inelastic spheres*. Arch. Ration. Mech. Anal., 87 (1985), 355–377.

[36] H. N. Latter, G. I. Ogilvie. *The linear stability of dilute particulate rings*. Icarus, 184 (2006), 498–516.

[37] H. N. Latter, G. I. Ogilvie. *Dense planetary rings and the viscous overstability*. Icarus, 195 (2008), 725–751.

[38] H. N. Latter, G. I. Ogilvie. *The viscous overstability, nonlinear wavetrains, and finescale structure in dense planetary rings*. Icarus, 202 (2009), 565–583.

[39] H. N. Latter, G. I. Ogilvie. *Hydrodynamical simulations of viscous overstability in Saturn's rings*. Icarus, 210 (2010), 318–329.

[40] M. C. Lewis, G. R. Stewart. *Collisional Dynamics of Perturbed Planetary Rings. I.* Astronomical Journal, 120 (2000), 3295–3310.

[41] D. N. C. Lin, P. Bodenheimer. *On the stability of Saturn's rings*. Astrophysical Journal, 248 (1981), L83–L86.

[42] D. N. C. Lin, J. E. Pringle. *A viscosity prescription for a self-gravitating accretion disc*. Monthly Notices Royal Astron. Soc., 225 (1987), 607–613.

[43] J. J. Lissauer, F. H. Shu, J. N. Cuzzi. *Moonlets in Saturn's rings*. Nature, 292 (1981), 707–711.

[44] P.-Y. Longaretti. *Saturn's main ring particle size distribution - an analytic approach*. Icarus, 81 (1989), 51–73.

[45] D. Lynden-Bell, J. Pringle. *The evolution of viscous discs and the origin of the nebular variables*. Mon.Not.Roy.Astron.Soc, 168 (1974), 603–637.

[46] J.-M. Petit, M. Henon. *A numerical simulation of planetary rings. III - Mass segregation, ring confinement, and gap formation*. Astronomy and Astrophysics, 199 (1988), 343–356.

[47] C. C. Porco. *S/2005 S 1*. IAU Circ., 8524 (2005), 1.

[48] J. E. Pringle. *Accretion discs in astrophysics*. Ann. Rev. Astron. Astrophys., 19 (1981), 137–162.

[49] J. Salmon, S. Charnoz, A. Crida, A. Brahic. *Long-term and large-scale viscous evolution of dense planetary rings*. Icarus, 209 (2010), 771–785.

[50] H. Salo. *Numerical simulations of dense collisional systems*. Icarus, 90 (1991), 254–270.

[51] H. Salo. *Gravitational wakes in Saturn's rings*. Nature, 359 (1992), 619–621.

[52] H. Salo. *Simulations of dense planetary rings. III. Self-gravitating identical particles.* Icarus, 117 (1995), 287–312.

[53] H. Salo, J. Schmidt, F. Spahn. *Viscous Overstability in Saturn's B Ring. I. Direct Simulations and Measurement of Transport Coefficients*. Icarus, 153 (2001), 295–315.

[54] J. Schmidt, H. Salo. *Weakly Nonlinear Model for Oscillatory Instability in Saturn's Dense Rings*. Physical Review Letters, 90 (2003), 6, 061102.

[55] J. Schmidt, H. Salo, F. Spahn, O. Petzschmann. *Viscous Overstability in Saturn's B-Ring. II. Hydrodynamic Theory and Comparison to Simulations*. Icarus, 153 (2001), 316–331.

[56] U. Schmit, W. M. Tscharnuter. *A fluid dynamical treatment of the common action of self-gravitation, collisions, and rotation in Saturn's B-ring.* Icarus, 115 (1995), 304–319.

[57] M. Seiß. *Moonlets in Saturn's dense rings*. PhD thesis (2009).

[58] M. Seiß, F. Spahn, M. Sremčević, H. Salo. *Structures induced by small moonlets in Saturn's rings: Implications for the Cassini Mission*. Geophysical Research Letters, 32 (2005), 11205.

[59] M. R. Showalter. *Visual detection of 1981S13, Saturn's eighteenth satellite, and its role in the Encke gap*. Nature, 351 (1991), 709–713.

[60] M. R. Showalter, J. N. Cuzzi, E. A. Marouf, L. W. Esposito. *Satellite 'wakes' and the orbit of the Encke Gap moonlet*. Icarus, 66 (1986), 297–323.

[61] F. H. Shu, L. Dones, J. J. Lissauer, C. Yuan, J. N. Cuzzi. *Nonlinear spiral density waves - Viscous damping*. Astrophysical Journal, 299 (1985), 542–573.

[62] I. G. Shukhman. *Collisional Dynamics of Particles in Saturn's Rings*. Sov. Astron., 28 (1984), 574.

[63] F. Spahn. *Scattering properties of a moonlet (satellite) embedded in a particle ring - Application to the rings of Saturn*. Icarus, 71 (1987), 69–77.

[64] F. Spahn, N. Albers, M. Sremcevic, C. Thornton. *Kinetic description of coagulation and fragmentation in dilute granular particle ensembles*. Europhysics Letters, 67 (2004), 545–551.

[65] F. Spahn, J. Schmidt, O. Petzschmann, H. Salo. *Note: Stability analysis of a Keplerian disk of granular grains: Influence of thermal diffusion*. Icarus, 145 (2000), 657–660.

[66] F. Spahn, H. Scholl, J. Hertzsch. *Structures in planetary rings caused by embedded moonlets*. Icarus, 111 (1994), 514–535.

[67] F. Spahn, H. Sponholz. *Existence of moonlets in Saturn's rings inferred from the optical depth profile*. Nature, 339 (1989), 607–608.

[68] F. Spahn, M. Sremčević. *Density patterns induced by small moonlets in Saturn's rings?* Astronomy and Astrophysics, 358 (2000), 368–372.

[69] F. Spahn, H.-J. Wiebicke. *Long-term gravitational influence of moonlets in planetary rings*. Icarus, 77 (1989), 124–134.

[70] M. Sremcevic, G. R. Stewart, N. Albers, J. E. Colwell, L. W. Esposito. *Density Waves in Saturn's Rings: Non-linear Dispersion and Moon Libration Effects*. Bulletin of the American Astronomical Society, 40 (2008), 430.

[71] M. Sremčević, J. Schmidt, H. Salo, M. Seiß, F. Spahn, N. Albers. *A belt of moonlets in Saturn's A ring*. Nature, 449 (2007), 1019–1021.

[72] M. Sremčević, F. Spahn, W. J. Duschl. *Density structures in perturbed thin cold discs*. Monthly Notices Royal Astron. Soc., 337 (2002), 1139–1152.

[73] G. R. Stewart, D. N. C. Lin, P. Bodenheimer. *Collision-induced transport processes in planetary rings*. Planetary Rings (R. Greenberg & A. Brahic, editor) (1984), 447–512.

[74] F. S. Thomson, E. A. Marouf, G. L. Tyler, R. G. French, N. J. Rappoport. *Periodic microstructure in Saturn's rings A and B*. Geophysical Research Letters, 34 (2007), 24203.

[75] M. S. Tiscareno, J. A. Burns, M. M. Hedman, C. C. Porco, *The Population of Propellers in Saturn's A Ring*. Astronomical Journal, 135 (2008), 1083–1091.

[76] M. S. Tiscareno, J. A. Burns, M. M. Hedman, C. C. Porco, J. W. Weiss, L. Dones, D. C. Richardson, C. D. Murray, *100-metre-diameter moonlets in Saturn's A ring from observations of 'propeller' structures*. Nature, 440 (2006), 648–650.

[77] M. S. Tiscareno, J. A. Burns, P. D. Nicholson, M. M. Hedman, C. C. Porco. *Cassini imaging of Saturn's rings. II. A wavelet technique for analysis of density waves and other radial structure in the rings*. Icarus, 189 (2007), 14–34.

[78] M. S. Tiscareno, J. A. Burns, M. Sremčević, K. Beurle, M. M. Hedman, N. J. Cooper, A. J. Milano, M. W. Evans, C. C. Porco, J. N. Spitale, J. W. Weiss. *Physical Characteristics and Non-Keplerian Orbital Motion of "Propeller" Moons Embedded in Saturn's Rings*. Astrophysical Journal Letters, 718 (2010), L92–L96.

[79] W. R. Ward. *On the radial structure of Saturn's rings*. Geophysical Research Letters, 8 (1981), 641–643.

[80] S. J. Weidenschilling, C. R. Chapman, D. R. Davis, R. Greenberg. *Ring particles - Collisional interactions and physical nature*. Planetary Rings (1984) pages 367–415.

[81] J. Wisdom, S. Tremaine. *Local simulations of planetary rings*. Astronomical Journal, 95 (1988), 925–940.

[82] H. A. Zebker, E. A. Marouf, G. L. Tyler. *Saturn's rings - Particle size distributions for thin layer model*. Icarus, 64 (1985), 531–548.